SIAM J. APPL. MATH.
Vol. 64, No. 4, pp. 1294–1310

MODELLING ANNULAR MICROMIXERS*

JAMES P. GLEESON†, OLIVIA M. ROCHE†, JONATHAN WEST‡, AND ANNE GELB§

Abstract. Magnetohydrodynamic mixing of two fluids in an annular microchannel is modelled as a two-dimensional laminar convection-diffusion problem and examined using asymptotic analysis and numerical simulation. The time T required for mixing of a plug of solute depends on the Péclet number Pe and on the geometry of the annulus. Three scaling regimes are identified: purely diffusive, Taylor-dispersive, and convection-dominated; each has a characteristic power-law dependence of T upon Pe. Consequences of these results for optimal micromixer design are discussed.

Key words. laminar mixing, convection-diffusion, asymptotic analysis, microfluidics

AMS subject classifications. 76M45, 76R99

DOI. 10.1137/S0036139902420407

1. Introduction. Recent advances in microfluidic and lab-on-a-chip technology have led to increased interest in laminar mixing of fluids [1, 2, 3]. Efficient mixing is vital for chemical reactions, but turbulence is absent at the low Reynolds numbers common in microscale devices, and molecular diffusion mixes on an unacceptably slow timescale. In this paper we discuss the mathematical modelling of an annular magnetohydrodynamic (MHD) micromixer, prototypes of which are under development at the Irish National Microelectronics Research Centre [4]. The device consists of an annular channel (see Figures 1 and 2), with inner and outer walls acting as electrodes and with an electromagnet underneath, which provides a vertical magnetic field. A radial electric field is imposed by applying a potential difference across the inner and outer electrodes, and the electric and magnetic fields produce an azimuthal Lorentz force, which acts as a pumping mechanism for the fluid [5].

The idealized mixing action of this device is illustrated in Figure 1: in the absence of molecular diffusion, the initially separated fluids are convected through each other, increasing the interfacial length between them (linearly in time), and so promoting the mixing action of diffusion. In reality, the actions of convection and diffusion are felt simultaneously, and the goal of this paper is to examine their effect upon the efficiency of the mixer. The discussion here is limited to two dimensions, where the idealized limit of infinite depth has been taken. Previous studies of MHD pumping in an annulus have been motivated by liquid-metal flows and their stability [5, 6], but to our knowledge this is the first investigation of the mixing effects in an annular geometry.

2. Notation and equations. The geometry of the annulus is shown in Figure 2. The radius of the center-line is R, and ρ represents the half-width of the channel; thus the inner wall is located at $r = R - \rho$, and the outer wall at $r = R + \rho$. We describe the geometry using the nondimensional parameter

*Received by the editors December 20, 2002; accepted for publication (in revised form) October 1, 2003; published electronically May 5, 2004. This work was funded by Science Foundation Ireland under Investigator Award 02/IN.1/IM062, the Enterprise Ireland International Collaboration Fund, the National Microelectronics Research Centre, and the Faculty of Arts Research Fund, University College Cork.

http://www.siam.org/journals/siap/64-4/42040.html

†Applied Mathematics, University College Cork, Ireland (j.gleeson@ucc.ie).

‡National Microelectronics Research Centre, Lee Maltings, Cork, Ireland (jonathan.west@newcastle.ac.uk).

§Department of Mathematics, Arizona State University, Tempe, AZ 85287 (ag@math.la.asu.edu).

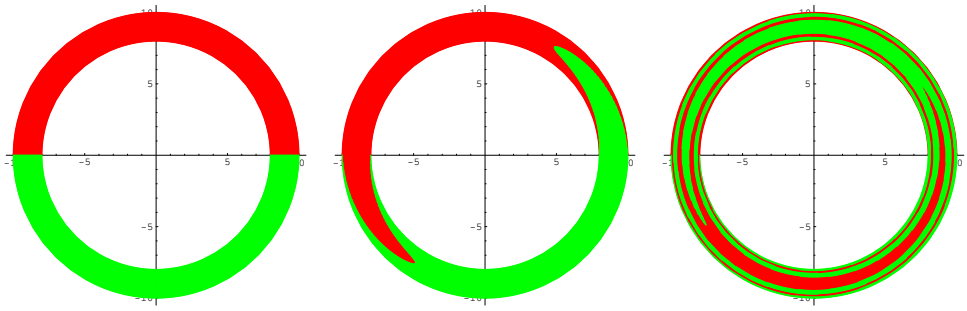

FIG. 1. *Operation of an idealized micromixer at three times, neglecting diffusion.*

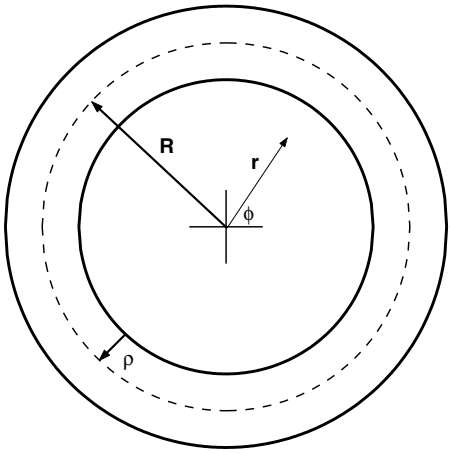

FIG. 2. *Annular geometry, showing the center-line radius R and the channel half-width ρ.*

$$\gamma = \frac{\rho}{R}, \tag{1}$$

which satisfies $0 < \gamma < 1$. Note that the limit $\gamma \to 0$ corresponds to a locally straight channel, and γ approaches 1 as the annulus becomes a punctured disk.

The fluid velocity in the micromixer is found by solving the steady Navier–Stokes equations in the presence of the MHD body force [6]. In the two-dimensional case considered here, this reduces to an ordinary differential equation for the azimuthal velocity $v(r)$, all other velocity components being zero:

$$\frac{d^2v}{dr^2} + \frac{1}{r}\frac{dv}{dr} - \frac{v}{r^2} = -\frac{\alpha}{r}, \tag{2}$$

where α represents the MHD forcing (specifically, $\alpha = -BI/4\pi h\eta$, where I and B are the root-mean-square current and magnetic field strengths, h is the channel depth, and η is the absolute viscosity of the fluid). The solution of (2) satisfying no-slip boundary conditions at the walls $r = R - \rho$ and $r = R + \rho$ is

$$v(r) = \frac{\omega}{8R\rho r}\left[\frac{1}{4} - \frac{(R^2-\rho^2)^2}{16R^2\rho^2}\left(\ln\frac{R-\rho}{R+\rho}\right)^2\right]^{-1} \times \left[(R^2-\rho^2)^2 \ln\frac{R-\rho}{R+\rho} + r^2(R-\rho)^2 \ln\frac{r}{R-\rho} + r^2(R+\rho)^2 \ln\frac{R+\rho}{r}\right], \tag{3}$$

where the velocity is characterized by an average angular velocity ω, which is related to the MHD forcing parameter α by

$$\omega = \alpha \left[\frac{1}{4} - \frac{(R^2 - \rho^2)^2}{16 R^2 \rho^2} \left(\ln \frac{R - \rho}{R + \rho} \right)^2 \right]. \tag{4}$$

The profile (3) reduces to the parabolic Poiseuille profile for a straight channel when $\gamma \to 0$,

$$v(r) \approx \frac{3\omega R}{2\rho^2}(r - R + \rho)(R + \rho - r), \tag{5}$$

with maximum at $r = R$:

$$v_{\max} = \frac{3}{2}\omega R. \tag{6}$$

The mixing of a plug of solute into a surrounding solvent is governed by the convection-diffusion equation (assuming both fluid phases have similar density, viscosity, etc.)

$$\frac{\partial c}{\partial t} + \nabla \cdot (\mathbf{u} c) - \kappa \nabla^2 c = 0, \tag{7}$$

where $\mathbf{u}(\mathbf{x}, t)$ is the fluid velocity vector, $c(\mathbf{x}, t)$ is the concentration of the solvent, and κ is the molecular diffusion coefficient. In the annular micromixer the convection-diffusion equation may be written in polar coordinates,

$$\frac{\partial c}{\partial t} + \frac{v(r)}{r}\frac{\partial c}{\partial \phi} - \frac{\kappa}{r}\frac{\partial}{\partial r}\left(r \frac{\partial c}{\partial r} \right) - \frac{\kappa}{r^2}\frac{\partial^2 c}{\partial \phi^2} = 0, \tag{8}$$

with no-flux boundary conditions at the walls:

$$\begin{aligned} \frac{\partial c}{\partial r}(R - \rho, \phi, t) &= 0, \\ \frac{\partial c}{\partial r}(R + \rho, \phi, t) &= 0. \end{aligned} \tag{9}$$

In the following sections we examine solutions of (8) using analytical, asymptotic, and numerical methods.

The dimensionless parameter used to compare the importance of convection and diffusion in (7) is the Péclet number, which we define for our system as

$$Pe = \frac{\omega R \rho}{\kappa}. \tag{10}$$

Note that ωR is the characteristic linear velocity, while ρ is the smallest linear dimension in the system. Two natural groupings of parameters to give a dimensional time will be used in what follows: the diffusion time R^2/κ, which measures the time for azimuthal mixing by diffusion in the absence of convection, and the convection time ω^{-1}, which is representative of the timescale of rotation of the fluid. The choice of appropriate time-scaling depends on whether diffusion or convection is dominant—we initially choose ω^{-1} but will consider the alternative in section 6.

A completely mixed solute-solvent system has the initial concentration $c(\mathbf{x}, 0)$ of solute spread evenly over the whole annulus. We define mixing efficiency using the timescale over which the concentration profile evolves to the uniform state. In order to measure the deviation from uniformity, we first introduce two averaging procedures, each operating on a function $f(r, \phi)$ defined on the annulus. Radial averaging is denoted by an overbar,

$$\overline{f} = \frac{1}{2R\rho} \int_{R-\rho}^{R+\rho} f(r, \phi) r dr, \tag{11}$$

and angle brackets signify angular averaging,

$$\langle f \rangle = \frac{1}{2\pi} \int_0^{2\pi} f(r, \phi) d\phi. \tag{12}$$

Thus the average value of the concentration over the whole annulus is

$$\langle \overline{c} \rangle = \frac{1}{4\pi R\rho} \int_{R-\rho}^{R+\rho} \int_0^{2\pi} c(r, \phi, t) r \, d\phi \, dr. \tag{13}$$

In fact, it is straightforward to show from the convection-diffusion equation that $\langle \overline{c} \rangle$ is a constant—the total amount of solute is not changed over time but is simply redistributed evenly over the annulus.

In the following sections we adopt a simple initial concentration,

$$c(r, \phi, 0) = 1 + \cos \phi, \tag{14}$$

for ease of asymptotic analysis. Later we show that the asymptotic results also apply to other initial conditions, for instance to the condition used in Figure 1:

$$c(r, \phi, 0) = \begin{cases} 1 & \text{if } 0 \le \phi < \pi, \\ 0 & \text{if } \pi \le \phi < 2\pi. \end{cases} \tag{15}$$

A *mixing measure* $m(t)$ is a positive function of time characterizing the deviation of the concentration at time t from its uniformly mixed state $\langle \overline{c} \rangle$. Define $m(t)$ by

$$m(t) = \frac{\left\langle \overline{(c(r, \phi, t) - \langle \overline{c} \rangle)^2} \right\rangle}{\left\langle \overline{(c(r, \phi, 0) - \langle \overline{c} \rangle)^2} \right\rangle}, \tag{16}$$

so that $m(0) = 1$, and $m(t) \to 0$ as $t \to \infty$. The time T_M for $m(t)$ to decay from 1 to a specified value M is called the *mixing time* and is defined by the condition

$$m(T_M) = M. \tag{17}$$

From the point of view of experimentalists and design engineers, it is desirable to have simple formulas relating the mixing time T_M to the Péclet number Pe and the geometry ratio γ of the micromixer. We proceed to obtain asymptotic approximations to the solution of (8), and hence scaling laws for the mixing times T_M.

3. Low Péclet numbers. When the Péclet number (10) is sufficiently small, diffusive effects completely dominate convective motion. The mixing time by diffusion alone may be calculated by solving the diffusion equation

$$\frac{\partial c}{\partial t} - \frac{\kappa}{r}\frac{\partial}{\partial r}\left(r\frac{\partial c}{\partial r}\right) - \frac{\kappa}{r^2}\frac{\partial^2 c}{\partial \phi^2} = 0 \tag{18}$$

in the annulus, i.e., neglecting the convective term in (8). A series solution can be written as

$$c = \langle \bar{c} \rangle + \sum_{n=1}^{\infty}\sum_{j=1}^{\infty} e^{-\kappa\lambda_{nj}t} G_n\left(r\sqrt{\lambda_{nj}}\right)\left[\alpha_{nj}\cos(n\phi) + \beta_{nj}\sin(n\phi)\right], \tag{19}$$

where the α_{nj} and β_{nj} are constants (determined from the initial condition) and λ_{nm} are eigenvalues determined by the conditions

$$\frac{dG_n}{dr} = 0 \quad \text{at } r = R-\rho \text{ and } r = R+\rho. \tag{20}$$

The eigenfunctions G_n are given in terms of Bessel functions as

$$G_n(r\sqrt{\lambda}) = J_n(r\sqrt{\lambda}) - Y_n(r\sqrt{\lambda})\left[\frac{J_{n-1}\left((R-\rho)\sqrt{\lambda}\right) - J_{n+1}\left((R-\rho)\sqrt{\lambda}\right)}{Y_{n-1}\left((R-\rho)\sqrt{\lambda}\right) - Y_{n+1}\left((R-\rho)\sqrt{\lambda}\right)}\right]. \tag{21}$$

For the single-mode initial condition (14), only the $n = 1$ term of the double sum is present in (19). Consequently, the mixing measure (16) in this case is

$$m(t) = \sum_{j=1}^{\infty} e^{-2\kappa\lambda_{1j}t}\frac{\overline{G_1\left(r\sqrt{\lambda_{1j}}\right)}^2}{\overline{G_1\left(r\sqrt{\lambda_{1j}}\right)}^2}. \tag{22}$$

The form of $m(t)$ at large times t is dominated by the first term ($j = 1$) in this sum. Indeed, in the limit $\gamma \to 0$, we have

$$m(t) \sim \exp(-2\kappa\lambda_{11}t) \quad \text{as } t \to \infty, \tag{23}$$

with the eigenvalue given by

$$\lambda_{11} = \frac{1}{R^2}\left[1 + \frac{1}{3}\gamma^2 + O(\gamma^4)\right] \text{ for } \gamma \ll 1. \tag{24}$$

The asymptotic mixing time T_M as defined in (17) then follows from (23) and (24),

$$T_M \sim \frac{1}{2\kappa\lambda_{11}}\ln\left(\frac{1}{M}\right) \quad \text{as } M \to 0, \tag{25}$$

and so the nondimensional mixing time is

$$\omega T_M \approx \frac{Pe}{2\gamma}\ln\left(\frac{1}{M}\right)\left[1 - \frac{1}{3}\gamma^2 + \cdots\right] \quad \text{for } \gamma \ll 1. \tag{26}$$

4. Intermediate Péclet numbers. In this section we follow and adapt Taylor's arguments [7] (see also [8]) to derive an effective dispersion under certain conditions on the Péclet number, and we clearly identify the limits of validity. We note that Nunge, Lin, and Gill [9] have derived a Taylor dispersion coefficient in a curved channel (matching our (35)), but they do not investigate for which values of Pe the analysis is valid. These bounding values of Pe assume great importance in our later analysis, so we follow Taylor's original formulation to understand when the approximations break down.

Consider a reference frame rotating with angular velocity ω, i.e., with azimuthal angle measured by

$$\phi' = \phi - \omega t. \tag{27}$$

The convection-diffusion equation (8) in this rotating frame is

$$\frac{\partial c}{\partial t} + \left(\frac{v(r)}{r} - \omega\right)\frac{\partial c}{\partial \phi'} - \frac{\kappa}{r}\frac{\partial}{\partial r}\left(r\frac{\partial c}{\partial r}\right) - \frac{\kappa}{r^2}\frac{\partial^2 c}{\partial \phi'^2} = 0, \tag{28}$$

with boundary conditions as before. We will work in this rotating frame for the remainder of this section and thus drop the prime on ϕ. Following Taylor, we assume that the concentration is quasi-steady in the rotating frame, with angular gradient $\frac{\partial c}{\partial \phi}$ independent of r. Moreover, the effect of azimuthal diffusion is neglected compared to radial diffusion. The resulting equation is readily integrated twice to yield

$$c = c(R-\rho,\phi) + \frac{1}{\kappa}\frac{\partial c}{\partial \phi}\int_{R-\rho}^{r}\frac{1}{r_2}\int_{R-\rho}^{r_2}\left[v(r_1) - \omega r_1\right] dr_1\, dr_2. \tag{29}$$

We take the radial mean (as defined in (11)) to allow us to eliminate $c(R-\rho,\phi)$ and obtain

$$c = \overline{c} + \frac{1}{\kappa}\frac{\partial c}{\partial \phi}\left[g(r) - \overline{g}\right], \tag{30}$$

having used the notation

$$g(r) = \int_{R-\rho}^{r}\frac{1}{r_2}\int_{R-\rho}^{r_2}\left[v(r_1) - \omega r_1\right] dr_1\, dr_2 \tag{31}$$

for brevity. The average flux of solvent through the line $\phi =$ constant (in the moving frame) is given by the radial average of the product of the concentration and angular velocity ω' (also relative to the moving frame):

$$\begin{aligned}\overline{J} &= \overline{c\,\omega'} \\ &= \frac{1}{2R\rho}\int_{R-\rho}^{R+\rho}\left[\overline{c} + \frac{1}{\kappa}\frac{\partial c}{\partial \phi}\left(g(r) - \overline{g}\right)\right]\left[\frac{v}{r} - \omega\right] r\, dr \\ &= \frac{1}{\kappa}\frac{\partial c}{\partial \phi}\frac{1}{2R\rho}\int_{R-\rho}^{R+\rho}\left(v(r) - \omega r\right) g(r) dr. \end{aligned} \tag{32}$$

If we assume

$$\frac{\partial c}{\partial \phi} \approx \frac{\partial \overline{c}}{\partial \phi}, \tag{33}$$

this implies that the radial mean concentration in the moving frame is governed by a one-dimensional diffusion equation

$$\frac{\partial \overline{c}}{\partial t} = D \frac{\partial^2 \overline{c}}{\partial \phi^2}, \tag{34}$$

where D is the Taylor dispersion coefficient for the annulus, defined by

$$\begin{aligned} D &= \frac{1}{\kappa} \frac{1}{2R\rho} \int_{R-\rho}^{R+\rho} (v(r) - \omega r)\, g(r)\, dr \\ &= \frac{1}{\kappa} \frac{1}{2R\rho} \int_{R-\rho}^{R+\rho} (v(r) - \omega r) \int_{R-\rho}^{r} \frac{1}{r_2} \int_{R-\rho}^{r_2} [v(r_1) - \omega r_1]\, dr_1\, dr_2\, dr. \end{aligned} \tag{35}$$

This integral may be calculated for the velocity (3); after some algebra we find

$$\begin{aligned} D = {} & \frac{\omega^2 R^2}{24\kappa\gamma} \left[4\gamma^2 - (1-\gamma^2)^2 \ln\left(\frac{1-\gamma}{1+\gamma}\right) \right]^{-2} \\ & \times \left[48\gamma^5(1+\gamma^2) + 120\gamma^4(1-\gamma^2)^2 \ln\frac{1+\gamma}{1-\gamma} - 72\gamma^3(1-\gamma^2)^2(1+\gamma^2) \left(\ln\frac{1+\gamma}{1-\gamma}\right)^2 \right. \\ & \left. - 6\gamma(1-\gamma^2)^4(1+\gamma^2) \left(\ln\frac{1+\gamma}{1-\gamma}\right)^4 + (1-\gamma^2)^4(3+10\gamma^2+3\gamma^4) \left(\ln\frac{1+\gamma}{1-\gamma}\right)^5 \right]. \end{aligned} \tag{36}$$

In the $\gamma \ll 1$ limit, this reduces to

$$D \approx \omega Pe \left[\frac{2}{105}\gamma + \frac{346}{1576}\gamma^3 \cdots \right]. \tag{37}$$

The solution of the one-dimensional diffusion equation (34) with initial condition from (14) is straightforward. Having found $\overline{c}$, we can calculate the concentration c and thus the mixing measure $m(t)$ from (30) and (16), respectively. The mixing measure has an exponential tail,

$$m(t) \sim \exp(-2Dt) \quad \text{as } t \to \infty, \tag{38}$$

and so the mixing time T_M is

$$T_M \sim \frac{1}{2D} \ln\left(\frac{1}{M}\right) \quad \text{as } M \to 0 \tag{39}$$

in the Taylor dispersion regime. From (37), this yields the (nondimensional) asymptotic form

$$\omega T_M \approx \frac{1}{\gamma Pe} \ln\left(\frac{1}{M}\right) \frac{105}{4} \left[1 - \frac{18165}{1576}\gamma^2 + \cdots \right] \text{ for } \gamma \ll 1 \tag{40}$$

when the assumptions made above are valid.

The range of Pe for which the above approximate analysis holds will prove to be of great interest in later sections, so we now examine carefully the two basic assumptions that were made and cast these into conditions on Pe for the result (40) to hold.

The first condition stems from the requirement that the azimuthal diffusion be negligible compared to the radial diffusion; effectively, this requires that the coefficient

of $\frac{\partial^2 c}{\partial \phi^2}$ in (28), actually its radial average, should be much less than the dispersion coefficient (35):

$$\kappa \ll D\overline{r^2}. \tag{41}$$

Consider this condition when $\gamma \ll 1$, using the first term of (37):

$$\begin{aligned} \kappa &\ll \frac{2}{105}\gamma\omega Pe R^2 \\ \iff Pe^2 &\gg \frac{105}{2}. \end{aligned} \tag{42}$$

The resulting condition $Pe \gg 7.2$ is analogous to that in a straight capillary; see, for instance, [8].

The second important approximation is the replacement of $\frac{\partial c}{\partial \phi}$ by $\frac{\partial \overline{c}}{\partial \phi}$ in (33). This is valid if the coefficient of $\frac{\partial c}{\partial \phi}$ in (30) is very small. The order of magnitude of this coefficient is $\overline{g}/\kappa$, and so the condition is

$$\frac{1}{\kappa}\frac{1}{2R\rho}\int_{R-\rho}^{R+\rho} r \int_{R-\rho}^{r} \frac{1}{r_2}\int_{R-\rho}^{r_2} [v(r_1) - \omega r_1]\, dr_1\, dr_2\, dr \ll 1. \tag{43}$$

Again, this yields a simple condition if $\gamma \ll 1$:

$$\begin{aligned} \frac{1}{15}\frac{\omega\rho^2}{\kappa} &\ll 1 \\ \iff Pe &\ll \frac{15}{\gamma}. \end{aligned} \tag{44}$$

Thus (42) and (44) provide rough bounds on Pe for the lower and upper ranges of validity of the Taylor dispersion approximations.

5. Convection-dominated mixing: $Pe \gg 1$. When molecular diffusion is small compared to convective effects, i.e., at large Péclet number, (8) is singularly perturbed. Mixing of a scalar at high Péclet numbers is a topic that has attracted much attention recently, with particular attention paid to the mixing of a passive scalar (as in our case), or vorticity (an active scalar), in the spiral flow field of a vortex [10, 11, 12]. In this section we apply approximation approaches based upon these works to understand the mixing speed in the annular micromixer.

As in previous sections, we examine the asymptotic limit of small γ, i.e., neglecting higher order effects of the channel curvature. Accordingly, (8) is rewritten using the nondimensional variables

$$\begin{aligned} \tilde{r} &= \frac{r-R}{\rho}, \\ \tilde{t} &= \omega t. \end{aligned} \tag{45}$$

Note that the nondimensional radial variable $\tilde{r}$ lies between -1 and 1, with $\tilde{r} = 0$ in the center of the channel. Taking the limit of small γ and using (5), equation (8) reduces to

$$\frac{\partial c}{\partial \tilde{t}} + \frac{3}{2}\left(1 - \tilde{r}^2\right)\frac{\partial c}{\partial \phi} - \epsilon\frac{\partial^2 c}{\partial \tilde{r}^2} = 0, \tag{46}$$

where $\epsilon = (\gamma Pe)^{-1}$ is a small parameter when Pe is sufficiently large.

It is well known [10, 11, 12] that scalar mixing occurs in vortex spiral flows on times scaling as $Pe^{1/3}$. Here we follow [10] to show that a similar scaling arises in the annular mixer, at least for early times. We consider the scalar evolving according to (46), and introduce the notation $\Omega(\tilde{r}) = 3/2(1-\tilde{r}^2)$ for the azimuthal velocity. In the complete absence of molecular diffusion, i.e., if $\epsilon = 0$, the evolution of the nth angular mode from an initial condition of

$$c(\tilde{t}=0) = \exp[in\phi] \tag{47}$$

is given by simple angular convection:

$$c = \exp\left[in\phi - in\Omega(\tilde{r})\tilde{t}\right]. \tag{48}$$

In order to include the effects of nonzero diffusion, we follow [10] and introduce a Lagrangian angular variable:

$$\theta = \phi - \Omega(\tilde{r})\tilde{t}. \tag{49}$$

The derivatives in (46) are then modified as follows:

$$\begin{aligned} \frac{\partial}{\partial \tilde{t}} &\to \frac{\partial}{\partial \tilde{t}} - \Omega\frac{\partial}{\partial\theta}, \\ \frac{\partial}{\partial \phi} &\to \frac{\partial}{\partial\theta}, \\ \frac{\partial}{\partial \tilde{r}} &\to \frac{\partial}{\partial \tilde{r}} - \Omega' \tilde{t}\frac{\partial}{\partial\theta}. \end{aligned} \tag{50}$$

Thus (46) becomes

$$\frac{\partial c}{\partial \tilde{t}} = \epsilon\left(\frac{\partial}{\partial \tilde{r}} - \Omega'\tilde{t}\frac{\partial}{\partial\theta}\right)^2 c, \tag{51}$$

and if the second term in parentheses dominates the first, we obtain

$$\frac{\partial c}{\partial \tilde{t}} = \epsilon\Omega'^2\tilde{t}^2\frac{\partial^2 c}{\partial\theta^2}. \tag{52}$$

The solution of this equation satisfying the initial condition (47) is

$$\begin{aligned} c &= \exp\left[in\theta - \epsilon n^2\Omega'^2\tilde{t}^3/3\right] \\ &= \exp\left[in\phi - in\Omega\tilde{t} - \epsilon n^2\Omega'^2\tilde{t}^3/3\right]. \end{aligned} \tag{53}$$

Noting that $\Omega' = -3\tilde{r}$ and $n = 1$ in our example, the mixing measure $m(t)$ can be calculated from (16) to yield (restoring dimensional variables)

$$m(t) = \frac{\sqrt{\pi}}{2}F\left(\frac{6\omega^3 t^3}{\gamma Pe}\right), \tag{54}$$

where F is defined as the monotonic function

$$F(x) = x^{-1/2}\mathrm{erf}(x^{1/2}). \tag{55}$$

The nondimensional mixing time corresponding to a mixing measure value of M is therefore

$$\omega T_M \approx \left[\frac{\gamma Pe}{6} F^{-1}\left(\frac{2M}{\sqrt{\pi}}\right)\right]^{1/3}, \tag{56}$$

and note in particular that this increases as $Pe^{1/3}$ when M and γ are fixed.

The approximation made to obtain (52) from (51) has limited validity, and so the $Pe^{1/3}$ scaling obtained in (56) is not expected to hold for all times. In particular, we note that $\Omega'(\tilde{r}) = 0$ at the center of the channel, and so (52) is not accurate there. An analogous situation was considered recently [13] for scalar mixing in a vortex: the vanishing azimuthal velocity at the center of the vortex is shown there to render the approximate solution (53) invalid at large times. A different approach is required: we follow [13] and [14] in seeking a solution of (46) of the form

$$c = g(\tilde{t}) \exp\left[in\phi - \frac{3}{2} in\tilde{t} - if(\tilde{t})\tilde{r}^2\right], \tag{57}$$

where the functions $g(\tilde{t})$ and $f(\tilde{t})$ are to be determined, subject to initial conditions $g(0) = 1$, $f(0) = 0$. This form for c can be motivated by noting that if $g \equiv 1$ and $f \equiv 0$, then (57) would be an exact solution of (46) if the azimuthal velocity Ω had no $\tilde{r}$-dependence. In fact, $f(\tilde{t})$ and $g(\tilde{t})$ can be found so that (57) is an exact solution of (46). Substituting (57) into (46) and taking $n = 1$ for the initial condition (14), we find first order equations for f and g:

$$\begin{aligned} \frac{df}{d\tilde{t}} &= -4i\epsilon f^2 - \frac{3}{2}, \\ \frac{dg}{d\tilde{t}} &= -2i\epsilon f g. \end{aligned} \tag{58}$$

Solutions satisfying the initial conditions are given by

$$\begin{aligned} f(\tilde{t}) &= \frac{3(1+i)}{2} \frac{1}{\mu} \tanh\left(\frac{-1+i}{2}\mu\tilde{t}\right), \\ g(\tilde{t}) &= \left[\cosh\left(\frac{-1+i}{2}\mu\tilde{t}\right)\right]^{-\frac{1}{2}}, \end{aligned} \tag{59}$$

where we have written $\mu = 2\sqrt{3\epsilon}$ for clarity. After some manipulation, using (57) in (16) yields a mixing measure

$$m = \sqrt{\frac{\pi}{6}}\mu \left[\sinh(\mu\tilde{t}) - \sin(\mu\tilde{t})\right]^{-\frac{1}{2}} \operatorname{erf}\left[\sqrt{\frac{3}{\mu}}\sqrt{\frac{\sinh(\mu\tilde{t}) - \sin(\mu\tilde{t})}{\cosh(\mu\tilde{t}) + \cos(\mu\tilde{t})}}\right]. \tag{60}$$

When $\mu\tilde{t} \ll 1$, this reduces to

$$\begin{aligned} m &\approx \sqrt{\frac{\pi}{2}} \left(\mu^2\tilde{t}^3\right)^{-\frac{1}{2}} \operatorname{erf}\left[\frac{1}{\sqrt{2}} \left(\mu^2\tilde{t}^3\right)^{\frac{1}{2}}\right] \\ &= \frac{\sqrt{\pi}}{2} F\left(\frac{6\omega^3 t^3}{\gamma Pe}\right), \end{aligned} \tag{61}$$

as in (54). The corresponding scaling for T_M is given by (56) and applies for values of M large enough so that $\mu\tilde{t} \ll 1$.

For $\mu\tilde{t} \gg 1$, the solution (60) decays exponentially in time:

$$m \approx \sqrt{\frac{\pi}{3}\mu}\,\mathrm{erf}\left[\sqrt{\frac{3}{\mu}}\right]\exp\left[-\frac{1}{2}\mu\tilde{t}\right], \tag{62}$$

and for large Péclet numbers $\mu \ll 1$, so the asymptotic mixing time is given (in dimensional variables) by

$$\omega T_M \approx \frac{1}{4}\sqrt{\frac{\gamma Pe}{3}}\ln\left[\frac{4\pi^2}{3M^4}\frac{1}{\gamma Pe}\right]. \tag{63}$$

Note that this mixing time scales as $Pe^{1/2}\ln Pe$ for fixed M and γ. This longer timescale replaces the $Pe^{1/3}$ scaling given by (56) when the mixing time T_M is sufficiently large that the $\mu\tilde{t} \gg 1$ asymptotics are important—this is relevant when we seek a level of mixing M that is sufficiently small. Physically, this new scaling emerges as a consequence of the vanishing of the differential rotation rate at the center of the channel: $\Omega'(0) = 0$; see [13] for a detailed discussion of the analogous problem at the vortex centers. Over short timescales (with $\mu\tilde{t} \ll 1$), the advective stretching and diffusion mix the scalar with time scaling as $Pe^{1/3}$. This convection-enhanced mixing is most effective near the sides of the channel, where the scalar is stretched into thin lamellae; see Figure 1(right-most panel). The more persistent scalar structure at the center of the channel is destroyed only on the longer timescales ($\mu\tilde{t} \gg 1$), leading to the $Pe^{1/2}\ln Pe$ scaling in (63). It is noteworthy that neither (53) nor (57) satisfy the no-flux boundary conditions (9) at the walls of the channel. However, numerical simulations (see section 6) indicate that this does not have an appreciable effect upon the accuracy of the asymptotic formulas. This is a consequence of the fast mixing of the scalar near the walls, so that any error in the boundary conditions is dominated by the slower-mixing scalar structure in the channel center.

6. Numerical simulations. To check the asymptotic results derived in previous sections, and to extend our analysis to cases with initial conditions other than the simple form (14), we solve the convection-diffusion equation (8) numerically. A decomposition into a finite number N of Fourier modes in the azimuthal angle is employed,

$$c(r,\phi,t) = \frac{1}{2}g_0(r,t) + \sum_{n=1}^{N} g_n(r,t)\cos(n\phi) + h_n(r,t)\sin(n\phi), \tag{64}$$

and substitution into (8) yields partial differential equations for g_n and h_n. Having solved the system of equations for the Fourier coefficients, the full concentration field may be constructed from (64), or the mixing measures may be evaluated more directly from (16) by integrating over the angle and normalizing $m(0)$ to unity:

$$m(t) = \overline{\left(\frac{g_0}{2} - \langle\overline{c}\rangle\right)^2 + \frac{1}{2}\sum_{n=1}^{N} g_n^2 + h_n^2}. \tag{65}$$

Logarithmic plots of $m(t)$ as a function of time at various Pe values are shown in Figure 3 for $\gamma = 0.05$. For comparison we plot also the asymptotic forms of $m(t)$, using (23) in the diffusive regime, (38) in the Taylor regime, and (54) and (60) in the convective regime. The asymptotic formulas fit the numerical results well, with

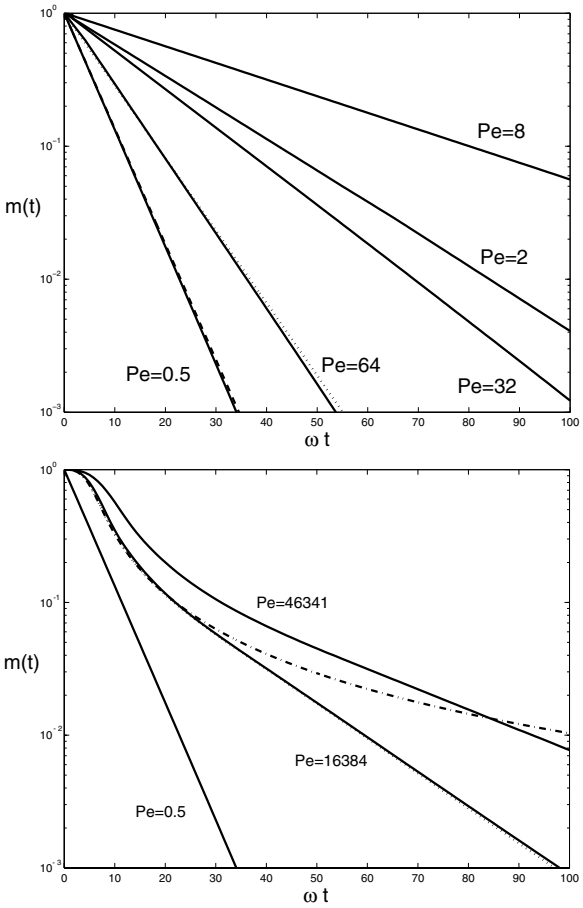

FIG. 3. *Mixing measure $m(t)$ as a function of nondimensional time, calculated in numerical simulations with $\gamma = 0.05$ and various Péclet numbers as shown. Asymptotic predictions are also shown for $Pe = 0.5$ (dashed) using* (23) *and $Pe = 64$ (dotted) using* (38) *in the upper panel. In the lower panel the asymptotic formulas* (54) *(dot-dash) and* (60) *(dotted) are shown for $Pe = 16384$.*

the exception of (54), which, as noted in section 5, is limited to early times. Taking account of the vanishing differential rotation rate at the center of the channel leads to (60), which matches the numerical results very well (the dotted line being almost indistinguishable from the solid).

From the numerical solution for $m(t)$, it is straightforward to calculate the mixing times T_M required for the measure to decay from its initial value of 1 to the value M. We choose three values of M for comparison with the asymptotic predictions—$M = 0.3$, 0.1, and 0.01—and investigate a wide range of Péclet numbers. For fixed values of γ and M, the asymptotic analysis of the previous sections predicts a mixing time proportional to Pe in the diffusion-dominated regime, to Pe^{-1} in the Taylor dispersion regime, and to either $Pe^{1/3}$ or $Pe^{1/2} \ln Pe$ when convection dominates. The numerical values of nondimensional times ωT_M are plotted in Figure 4 along with the straight lines corresponding to the formulas (26), (40), and (56) for all three values of M. Note the excellent agreement with predictions, except for the lowest value of M, when the approximation (54) no longer accurately describes the time evolution of $m(t)$. For this value of M the asymptotic result (63) is plotted with a dotted line and is found

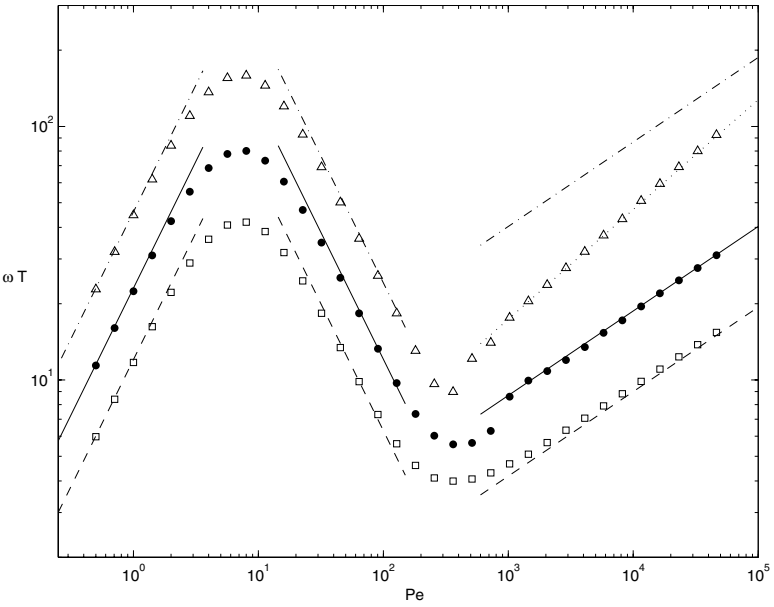

FIG. 4. *Nondimensional mixing times as a function of Péclet number, for* $\gamma = 0.05$. *Asymptotic results are shown as lines, and numerical results as symbols for values of the mixing measure:* $M = 0.3$ *(dashed line; squares),* $M = 0.1$ *(solid line, points), and* $M = 0.01$ *(dot-dash line, triangles). The long-time asymptotic result* (63) *is also plotted as a dotted line for the case of* $M = 0.01$.

to closely match the numerical results.

Because much of our analysis has concentrated on the $\gamma \to 0$ limit, it is worthwhile comparing numerics and asymptotics for a larger value of γ, noting that the maximum possible value of γ is 1. In Figure 5 we plot the results for $\gamma = 0.2$ and find that in general the correspondence between predicted and numerical values is excellent. However, we note that the limits on the Taylor regime now preclude the formation of a clear Pe^{-1} scaling range.

Another simplification in the analysis concerns the initial condition (14), which consists of only a single harmonic of the azimuthal variable. In order to examine the robustness of our predictions, we numerically solve the convection-diffusion equation for initial condition (15), replacing the discontinuous function by hyperbolic tangents to avoid Gibbs oscillations. The decay of the mixing measure is still dominated by the first angular harmonic, and so the mixing times are remarkably close to the asymptotic estimates; see Figure 6. We therefore expect the formulas to be useful for rather general initial distributions of the solute.

The nondimensional time ωT_M used in Figures 3–6 may be replaced by the alternative nondimensionalization mentioned in section 2, i.e., the diffusion time $\kappa T_M / R^2$. The timescales are related by

$$\frac{\kappa T_M}{R^2} = \frac{\gamma}{Pe}\,\omega T_M, \tag{66}$$

and so the data of, for example, Figure 4 is easily recast in terms of the diffusion time; see Figure 7. The relevant mixing times in the diffusive, Taylor, and convective

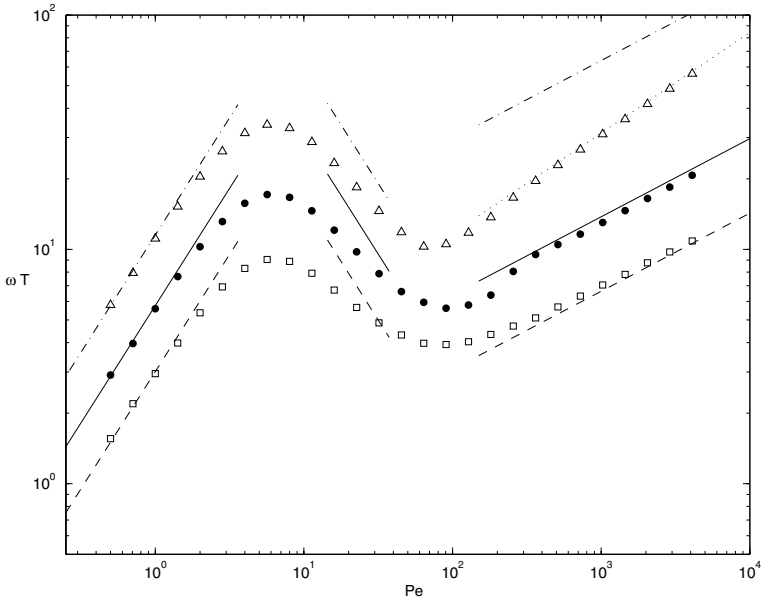

FIG. 5. *Nondimensional mixing times as a function of Péclet number for* $\gamma = 0.2$. *Asymptotic results are shown as lines, and numerical results as symbols for values of the mixing measure:* $M = 0.3$ *(dashed line; squares),* $M = 0.1$ *(solid line, points), and* $M = 0.01$ *(dot-dash line, triangles). The long-time asymptotic result* (63) *is also plotted as a dotted line for the case of* $M = 0.01$.

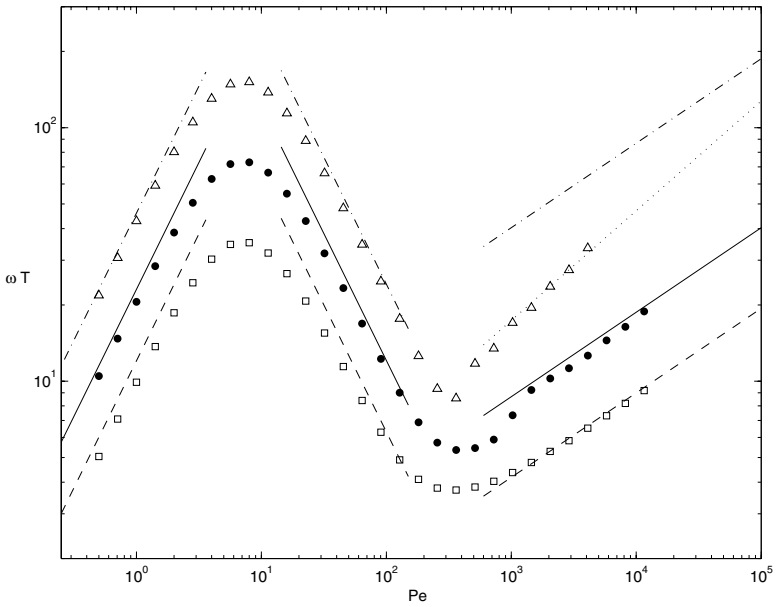

FIG. 6. *Nondimensional mixing times as a function of Péclet number, for* $\gamma = 0.05$ *and an initial concentration given by* (15) *(slightly smoothed). Asymptotic results are shown as lines, and numerical results as symbols for values of the mixing measure:* $M = 0.3$ *(dashed line; squares),* $M = 0.1$ *(solid line, points), and* $M = 0.01$ *(dot-dash line, triangles). The long-time asymptotic result* (63) *is also plotted as a dotted line for the case of* $M = 0.01$.

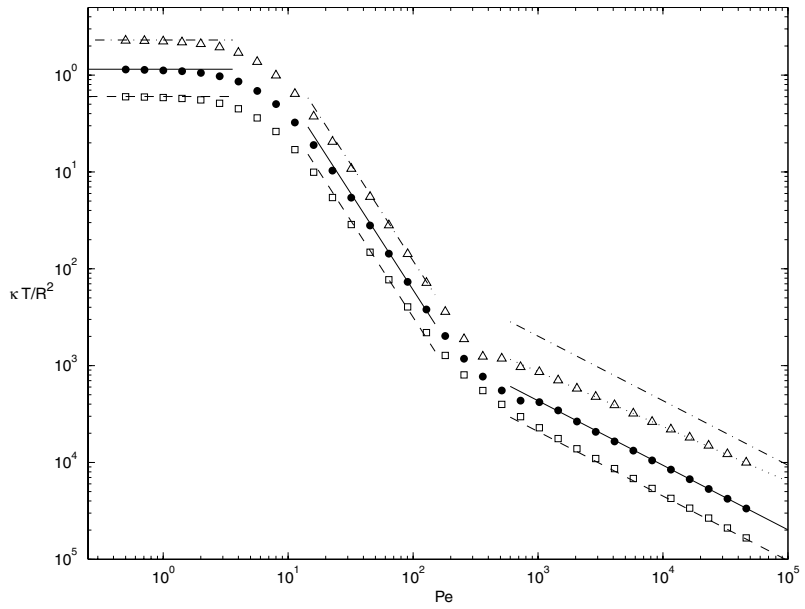

FIG. 7. *Mixing times nondimensionalized by the diffusion time, $\kappa T/R^2$, as a function of Péclet number, for $\gamma = 0.05$. Asymptotic results are shown as lines, and numerical results as symbols for values of the mixing measure: $M = 0.3$ (dashed line; squares), $M = 0.1$ (solid line, points), and $M = 0.01$ (dot-dash line, triangles). The long-time asymptotic result* (70) *is also plotted as a dotted line for the case of $M = 0.01$.*

regimes are thus found by multiplying (26), (40), (56), and (63) by γ/Pe, yielding

$$\frac{\kappa T_M}{R^2} \approx \frac{1}{2}\ln\left(\frac{1}{M}\right)\left[1 - \frac{1}{3}\gamma^2 + \cdots\right] \tag{67}$$

for $Pe \ll 7.2$ and

$$\frac{\kappa T_M}{R^2} \approx \frac{1}{Pe^2}\ln\left(\frac{1}{M}\right)\frac{105}{4}\left[1 - \frac{18165}{1576}\gamma^2 + \cdots\right] \tag{68}$$

for $7.2 \ll Pe \ll 15/\gamma$. For the highest Péclet numbers $Pe \gg 15/\gamma$, we obtained two asymptotic forms, the first valid for short times (moderate M values),

$$\frac{\kappa T_M}{R^2} \approx Pe^{-\frac{2}{3}}\gamma^{\frac{4}{3}}\left[\frac{1}{6}F^{-1}\left(\frac{2M}{\sqrt{\pi}}\right)\right]^{1/3}, \tag{69}$$

and the second for longer times (smaller M values),

$$\frac{\kappa T_M}{R^2} \approx Pe^{-\frac{1}{2}}\gamma^{\frac{3}{2}}\frac{1}{4\sqrt{3}}\ln\left[\frac{4\pi^2}{3M^4}\frac{1}{\gamma Pe}\right]. \tag{70}$$

Figure 7 is especially of interest to experimentalists working with a particular solute and solvent (so that κ is fixed) while varying the rate of rotation velocity ω of the micromixer to change Pe. The mixing time is seen to decrease from the diffusion time through the Taylor regime (at a rate proportional to Pe^{-2}), and then continue to decrease at a slower rate beyond the Taylor regime. The slower rate corresponds

to a $Pe^{-2/3}$ scaling when (54) is valid, i.e., for $M \geq 0.1$, but is closer to $Pe^{-1/2} \ln Pe$ for very small values of M.

From our analysis of the limits of validity of the Taylor dispersion description (see (44)), we can estimate the end of the Taylor regime as $15\gamma^{-1}$ for small γ. Of interest to the micromixer designer is the influence of the geometry ratio γ: since the mixing time decreases as Pe^{-2} until $Pe \approx 15\gamma^{-1}$, it seems advisable to decrease γ as much as possible in order to achieve faster mixing at lower velocities. However, this approach is overly simplistic, since the Péclet number also depends on γ—the linear velocity in the channel decreases with decreasing ρ, all other things being equal. A problem of great relevance to experimentalists is to find the optimal annular geometry to give the lowest possible mixing time for a given species, and given values of the electric and magnetic pumping fields (so κ and α are fixed). Suppose that the "footprint" R of the device is chosen; then we must find the channel half-width ρ to minimize the mixing time. Since Pe may be shown to increase monotonically with ρ, we conclude from Figure 7 that the mixing time decreases as the channel width increases. Practical considerations such as the minimal inner radius for effective electrodes will also provide an upper bound on the acceptable geometry ratio γ.

7. Summary. Laminar mixing in a two-dimensional annulus has been examined by asymptotic analysis and numerical simulation of the convection-diffusion equation (8). The mixing measure defined in (16) has been shown to decay exponentially in the diffusion and Taylor regimes (see (23) and (38)), with time constants given in terms of the Péclet number and the ratio γ characterizing the annulus geometry. Corresponding mixing times T_M are predicted to scale as Pe^0 and Pe^{-2} relative to the azimuthal diffusion time; see (67) and (68). Figures 3–7 demonstrate the robustness of these predictions by comparing them to numerical simulations. In the convection-dominated regime, asymptotic analysis modelled upon studies of mixing in vortices yields the mixing measure (60), with two interesting subregimes for the mixing time: a $Pe^{-2/3}$ dependence for early times, crossing over to a $Pe^{-1/2} \ln Pe$ scaling at longer times, as shown in (69) and (70), respectively. These predictions are again found to agree well with numerical results. Although the asymptotic formulas were derived in the limit $\gamma \to 0$, we find that they also yield good predictions for larger values of γ (Figure 5).

An important limitation of the present analysis is the assumption that all motion is two-dimensional; it is known [15, 16] that the dispersion in a channel of finite depth may not equal the value calculated by assuming the depth to be infinite. Work incorporating three-dimensional effects may yield further insight into this important problem.

Acknowledgment. We acknowledge the helpful comments of the anonymous referees.

REFERENCES

[1] J. P. Gleeson and J. West, *Magnetohydrodynamic micromixing*, in Proceedings of the Fifth International Conference on Modeling and Simulation of Microsystems 2002, Puerto Rico, Computational Publications, Cambridge, MA, 2002, pp. 318–321.

[2] I. Meisel and P. Ehrhard, *Simulation of electrically excited flows in microchannels for mixing application*, in Proceedings of the Fifth International Conference on Modeling and Simulation of Microsystems 2002, Puerto Rico, Computational Publications, Cambridge, MA, 2002, pp. 62–65.

[3] K. Mohseni, *Mixing and impulse extremization in microscale vortex formation*, in Proceedings of the Fifth International Conference on Modeling and Simulation of Microsystems 2002, Puerto Rico, Computational Publications, Cambridge, MA, 2002, pp. 392–395.
[4] J. West, B. Karamata, B. Lillis, J. P. Gleeson, J. Alderman, J. K. Collins, W. Lane, A. Mathewson, and H. Berney, *Application of magnetohydrodynamic actuation to continuous flow chemistry*, Lab on a Chip, 2 (2002), pp. 224–230.
[5] P. Tabeling and J. P. Chabrerie, *Magnetohydrodynamic Taylor vortex flow under a transverse pressure gradient*, Phys. Fluids, 24 (1981), pp. 406–412.
[6] M-H. Chang and C-K. Chen, *Hydromagnetic stability of current-induced flow in a small gap between concentric cylinders*, J. Fluids Engrg., 121 (1999), pp. 548–554.
[7] G. I. Taylor, *Dispersion of soluble matter in solvent flowing slowly through a tube*, Proc. Roy. Soc. London A, 219 (1953), pp. 186–203.
[8] R. F. Probstein, *Physiochemical Hydrodynamics*, Wiley, New York, 1994.
[9] R. J. Nunge, T.-S. Lin, and W. N. Gill, *Laminar dispersion in curved tubes and channels*, J. Fluid Mech., 51 (1972), pp. 363–383.
[10] D. I. Pullin and T. S. Lundgren, *Axial motion and scalar transport in stretched spiral vortices*, Phys. Fluids, 13 (2001), pp. 2553–2563.
[11] P. Flohr and J. C. Vassilicos, *Accelerated scalar dissipation in a vortex*, J. Fluid Mech., 348 (1997), pp. 295–317.
[12] P. B. Rhines and W. R. Young, *How rapidly is a passive scalar mixed within closed streamlines?*, J. Fluid Mech., 133 (1983), pp. 133–145.
[13] K. Bajer, A. P. Bassom, and A. D. Gilbert, *Accelerated diffusion in the centre of a vortex*, J. Fluid Mech., 437 (2001), pp. 395–411.
[14] M. J. Lighthill, *Initial development of diffusion in a Poiseuille flow*, J. Inst. Math. Appl., 2 (1966), pp. 97–108.
[15] H. Brenner and D. A. Edwards, *Macrotransport Processes*, Butterworth–Heinemann, Boston, 1993.
[16] M. R. Doshi, P. M. Daiya, and W. N. Gill, *Three dimensional laminar dispersion in open and closed rectangular conduits*, Chem. Eng. Sci., 33 (1978), pp. 795–804.